PAN ARCHIVES OF ACOUSTICS
Vol. 40, No. 3, pp. 311–319 (2015)

DOI: 10.1515/aoa-2015-0034

# Shape Optimization of Mufflers Composed of Multiple Rectangular Fin-Shaped Chambers Using Differential Evolution Method

Min-Chie CHIU[(1)], Ying-Chun CHANG[(2)], Ho-Chih CHENG[(1)], Wei-Ting TAI[(2)]

[(1)] *Department of Mechanical and Automation Engineering, Chung Chou University of Science and Technology*
6, Lane 2, Sec.3, Shanchiao Rd., Yuanlin, Changhua 51003, Taiwan, R.O.C.; e-mail: minchie.chiu@msa.hinet.net

[(2)] *Department of Mechanical Engineering, Tatung University*
No. 40, Sec. 3, Zhongshan N.Rd., Taipei 104, Taiwan, R.O.C.

(*received Aril 16, 2015; accepted May 22, 2015*)

There has been considerable research done on multi-chamber mufflers used in the elimination of industrial venting noise. However, most research has been restricted to lower frequencies using the plane wave theory. This has led to underestimating acoustical performances at higher frequencies. Additionally, because of the space-constrained problem in most plants, the need for optimization of a compact muffler seems obvious. Therefore, a muffler composed of multiple rectangular fin-shaped chambers is proposed.

Based on the eigenfunction theory, a four-pole matrix used to evaluate the acoustic performance of mufflers will be deduced. A numerical case for eliminating pure tones using a three-fin-chamber muffler will also be examined. To delineate the best acoustical performance of a space-constrained muffler, a numerical assessment using the Differential Evolution (*DE*) method is adopted. Before the *DE* operation for pure tone elimination can be carried out, the accuracy of the mathematical model must be checked using experimental data. The results reveal that the broadband noise has been efficiently reduced using the three-fin-chamber muffler.

Consequently, a successful approach in eliminating a pure tone using optimally shaped three-fin-chamber mufflers and a differential evolution method within a constrained space has been demonstrated.

**Keywords:** fin, multi-chamber, high-order-mode, differential evolution.

## Notations

This paper is constructed on the basis of the following notations:

$A$ – width of the expansion chamber [m],
$A_o$ – width of the fin-type chamber [m],
$a_1$ – width of the inlet [m],
$a_2$ – width of the outlet [m],
$(a_{c1}, b_{c1})$ – centre coordinate of the inlet [m],
$(a_{c2}, b_{c2})$ – centre coordinate of the outlet [m],
$b_1$ – height of the inlet [m],
$b_2$ – height of the outlet (m),
$CR$ – crossover rate in *DE*,
$c_o$ – sound speed [m/s],
$f$ – cyclic frequency [Hz],
$F$ – mutation factor in *DE*,
$H$ – height of the expansion chamber [m],
$H_o$ – height of the fin-type chamber [m],
$iter_{\max}$ – maximum iteration,
$j$ – imaginary unit,
$k$ – wave number ($= \omega/c_o$),
$L$ – width of the expansion chamber [m],
$L1$ – horizontal distance between the fins [m],
$NP$ – population number in *DE*,
$OBJ$ – objective function [dB],
$\overline{P}_1$ – acoustical potential energy at the inlet [Pa],
$\overline{P}_2$ – acoustical potential energy at the outlet [Pa],
$\overline{p}_{11}$, $\overline{p}_{22}$ – acoustical pressure at the normal direction for inlet and outlet [Pa],
$\overline{p}_{12}$, $\overline{p}_{21}$ – acoustical pressure at the tangent direction for inlet and outlet [Pa],
$S_0$ – section area of the expansion chamber [m$^2$],
$S_1$ – section area of the inlet [m$^2$],
$S_2$ – section area of the outlet [m$^2$],
$T1$ – thickness of the fin-type chamber [m],
$T_{ij}$, $T_{Tij}$ – components of a four-pole transfer system matrix,
$TL$ – sound transmission loss [dB],
$U_i$ – volume velocity [m/s],
$Z_0$ – acoustical impedance of the expansion chamber in $z$-axis,
$Z_1$ – acoustical impedance of the inlet in $z$-axis,
$Z_2$ – acoustical impedance of outlet in $z$-axis,
$\omega$ – angular frequency (radius/s).

## 1. Introduction

Most research on mufflers has been restricted to lower frequencies using the plane wave theory. Garashi, Toyama, Miwa, and Arai's prediction of a muffler's acoustical performance using a four-pole transfer matrix (Igarashi Toyama, 1958; Miwa Igarashi, 1959; Igarashi Arai, 1960) is an example. Because the solutions mentioned above were based on the plane wave theory, the acoustical effect of higher order waves was ignored. In order to overcome this shortcoming, Ih and Lee (1985, 1987), evaluated the acoustical performance of an expansion and circular-sectioned muffler at a high-order-mode. Munjal (1987) simplified the calculation process using a numerical analysis method; however, the ratio of the expansion area to the inlet/outlet area was limited to an integer value. Unfortunately, there is a difficulty in analyzing a muffler using the analytic method when the angle between the inlet and outlet is preset at 90 degrees. Abom (1990) proposed a four-pole matrix for an extended muffler with a circular section. Ih (1992) demonstrated a numerical technique for analyzing the noise reduction of an expansion muffler having a circular/rectangular section and an inlet/outlet duct. Also, because of the space-constrained problem for an existing plant, the optimization of a compact muffler is essential. However, shape optimization for a space-constrained muffler in a high-order-mode has been neglected. Moreover, the high-order wave analysis of a muffler using the finite element method (FEM) (Young, Crocker, 1975) or the two-dimensional boundary element method (BEM) (Seybert, Cheng, 1987) requires an enormous amount of time to establish the acoustical mode and calculate the sound fields. With this in mind, Chang and Chiu (2013; 2014a; 2014b) proposed a simplified ANN (Artificial Neural Network) model in conjunction with the FEM & BEM and the genetic method to find optimally shaped rectangular mufflers equipped with simple baffles. However, because of the complicated model built by the ANN, the number of designed parameters was limited. In order to overcome this drawback, Chiu and Chang (2014) analyzed the optimal shape of a rectangular expansion chamber using eigenfunction, which is an analytic solution. Here, the acoustical elimination was focused on a one-chamber rectangular muffler. As shown by Yeh *et al.* (2004), the number of simple-expansion chambers in a series can increase the acoustical performance. Therefore, in order to improve the acoustical performance within a constrain space, a muffler composed of three rectangular fin-shaped chambers is proposed in this paper.

Differential Evolution (*DE*) has been acknowledged as one of the best stochastic direct search methods. The classical gradient methods *EPFM IPFM* and *FDM* need good starting points (design data) when a global optimum is searched during the optimization (Chang *et al.*, 2005); therefore, the accuracy will be limited. Recently, the Genetic Algorithm (GA), one kind of the evolutionary algorithm used to search for the global optimum by imitating a genetic evolutionary process, has been widely applied in various fields (Chang *et al.*, 2004; Chiu, Chang, 2008; Chiu, 2010). However, there are many control parameters such as the population size, bit length of the chromosome, elitism, mutation rate, crossover rate, and maximum iteration in the GA optimization. In order to simplify the optimization procedure, a Differential Evolution (*DE*) method with fewer control parameters is adopted in the muffler optimization. Note that Differential Evolution (*DE*), a population-based search algorithm invented by Price and Storn (1995; 1997), uses a real-valued vector for the design variable and evaluates for optimization by using mutation, crossover, and selection. Therefore, no good starting point is required during the optimization process. To simplify the optimization procedure, a Differential Evolution (DE) method with fewer control parameters is adopted in the muffler optimization.

## 2. Theoretical background

### 2.1. Mathematical model for a straight rectangular muffler

As indicated in Fig. 1, concerning the higher order wave propagating along a rectangular muffler and assuming that a rigid rectangular tube is driven by a piston along the tube wall, the acoustical pressure of the inlet in the normal direction is (Ih, 1992):

$$\begin{aligned}\overline{p}_{11} &= (-1)^1 jU_1 Z_0 \left\{ \frac{1}{\tan kL} + \left(\frac{AH}{a_1 b_1}\right)^2 \right. \\ &\cdot \left[ \sum \frac{1}{v_{m0}} \left(\frac{2}{m\pi}\right)^2 \left(\frac{b_1}{H}\right)^2 \psi_{111}^2 \right. \\ &+ \sum \frac{1}{v_{0n}} \left(\frac{2}{n\pi}\right)^2 \left(\frac{a_1}{A}\right)^2 \psi_{211}^2 \\ &\left. \left. + \sum\sum \frac{1}{v_{mn}} \left(\frac{4}{mn\pi^2}\right)^2 \psi_{111}^2 \psi_{211}^2 \right] \frac{k}{k_z \tan k_z L} \right\} \\ &= (-1)^1 jU_1 Z_0 E_{11}, \end{aligned} \tag{1}_1$$

where

$$\begin{aligned} \psi_{111} &= \sin\frac{m\pi a_1}{2A} \cos\frac{m\pi a_{c1}}{A}, \\ \psi_{211} &= \sin\frac{m\pi b_1}{2H} \cos\frac{m\pi b_{c1}}{H}. \end{aligned} \tag{1}_2$$

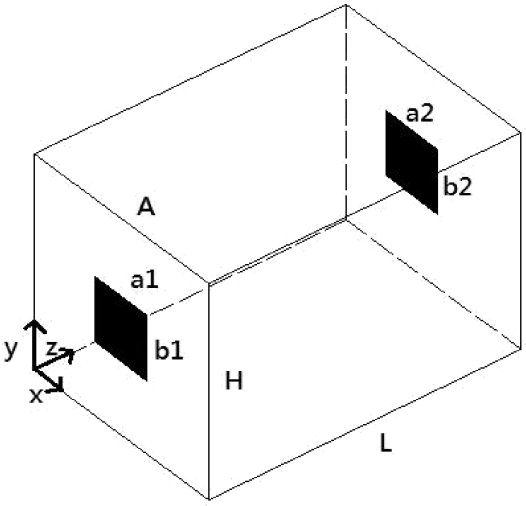


Fig. 1. Straight rectangular muffler.

In addition, the acoustical pressure of the outlet in the normal direction yields

$$\begin{aligned}\overline{p}_{22} &= (-1)^2 jU_2Z_0\left\{\frac{1}{\tan kL}+\left(\frac{AH}{a_2b_2}\right)^2\right.\\ &\cdot\left[\sum\frac{1}{v_{m0}}\left(\frac{2}{m\pi}\right)^2\left(\frac{b_2}{H}\right)^2\psi_{122}^2\right.\\ &+\sum\frac{1}{v_{0n}}\left(\frac{2}{n\pi}\right)^2\left(\frac{a_2}{A}\right)^2\psi_{222}^2\\ &\left.\left.+\sum\sum\frac{1}{v_{mn}}\left(\frac{4}{mn\pi^2}\right)^2\psi_{122}^2\psi_{222}^2\right]\frac{k}{k_z\tan k_zL}\right\}\\ &= (-1)^2 jU_2Z_0E_{22}, \qquad (2)_1\end{aligned}$$

where

$$\begin{aligned}\psi_{122} &= \sin\frac{m\pi a_2}{2A}\cos\frac{m\pi a_{c2}}{A},\\ \psi_{222} &= \sin\frac{m\pi b_2}{2H}\cos\frac{m\pi b_{c2}}{H}\end{aligned} \qquad (2)_2$$

and, the acoustical pressure of the inlet in a tangential direction yields

$$\begin{aligned}\overline{p}_{12} &= (-1)^2 jU_2Z_0\left\{\frac{1}{\sin kL}+\left(\frac{AH}{a_1b_1}\right)\left(\frac{AH}{a_2b_2}\right)\right.\\ &\cdot\left[\sum\frac{1}{v_{m0}}\left(\frac{2}{m\pi}\right)^2\left(\frac{b_1}{H}\right)\left(\frac{b_2}{H}\right)\psi_{112}\psi'_{112}\right.\\ &+\sum\frac{1}{v_{0n}}\left(\frac{2}{n\pi}\right)^2\left(\frac{a_1}{A}\right)\left(\frac{a_2}{A}\right)\psi_{212}\psi'_{212}\\ &\left.\left.+\sum\sum\frac{1}{v_{mn}}\left(\frac{4}{mn\pi^2}\right)^2\psi_{112}\psi'_{112}\psi_{212}\psi'_{212}\right]\right.\\ &\left.\cdot\frac{k}{k_z\sin k_zL}\right\} = (-1)^2 jU_2Z_0E_{12}, \qquad (3)_1\end{aligned}$$

$$\begin{aligned}\overline{p}_{21} &= (-1)^1 jU_1Z_0\left\{\frac{1}{\sin kL}+\left(\frac{AH}{a_2b_2}\right)\left(\frac{AH}{a_1b_1}\right)\right.\\ &\cdot\left[\sum\frac{1}{v_{m0}}\left(\frac{2}{m\pi}\right)^2\left(\frac{b_2}{H}\right)\left(\frac{b_1}{H}\right)\psi_{121}\psi'_{121}\right.\\ &+\sum\frac{1}{v_{0n}}\left(\frac{2}{n\pi}\right)^2\left(\frac{a_2}{A}\right)\left(\frac{a_1}{A}\right)\psi_{221}\psi'_{221}\\ &\left.\left.+\sum\sum\frac{1}{v_{mn}}\left(\frac{4}{mn\pi^2}\right)^2\psi_{121}\psi'_{121}\psi_{221}\psi'_{221}\right]\right.\\ &\left.\cdot\frac{k}{k_z\sin k_zL}\right\} = (-1)^1 jU_1Z_0E_{21}, \qquad (3)_2\end{aligned}$$

where

$$\begin{aligned}\psi_{121} &= \sin\frac{m\pi a_1}{2A}\cos\frac{m\pi a_{c1}}{A},\\ \psi_{112} &= \sin\frac{m\pi a_2}{2A}\cos\frac{m\pi a_{c2}}{A},\\ \psi'_{121} &= \sin\frac{m\pi a_2}{2A}\cos\frac{m\pi a_{c2}}{A},\\ \psi'_{112} &= \sin\frac{m\pi a_1}{2A}\cos\frac{m\pi a_{c1}}{A},\\ \psi_{221} &= \sin\frac{n\pi b_1}{2H}\cos\frac{n\pi b_{c1}}{H},\\ \psi_{212} &= \sin\frac{n\pi b_2}{2H}\cos\frac{n\pi b_{c2}}{H},\\ \psi'_{221} &= \sin\frac{n\pi b_2}{2H}\cos\frac{n\pi b_{c2}}{H},\\ \psi'_{212} &= \sin\frac{n\pi b_1}{2H}\cos\frac{n\pi b_{c1}}{H}.\end{aligned} \qquad (3)_3$$

Combining Eqs. (1)–(3) yields

$$\begin{aligned}\overline{P}_1 &= \overline{p}_{11}+\overline{p}_{12} = -jZ_0\left(U_1E_{11}-U_2E_{12}\right),\\ \overline{P}_2 &= \overline{p}_{21}+\overline{p}_{22} = -jZ_0\left(U_1E_{21}-U_2E_{22}\right).\end{aligned} \qquad (4)$$

Here, $\overline{P}_1$ is the total acoustical pressure of the inlet, and $\overline{P}_2$ is the total acoustical pressure of the outlet. Rearranging Eq. (4) into a matrix yields

$$\begin{bmatrix}P_1\\U_1\end{bmatrix} = \begin{bmatrix}T_{11} & T_{12}\\T_{21} & T_{22}\end{bmatrix}\begin{bmatrix}P_2\\U_2\end{bmatrix},$$

where

$$\begin{aligned}T_{11} &= \left(\overline{P}_1/\overline{P}_2\right)|_{U_2=0} = E_{11}/E_{12}\ ,\\ T_{12} &= \left(\overline{P}_1/U_2\right)|_{\overline{P}_2=0} = jZ_0(E_{12}E_{22}/E_{12})\ ,\\ T_{21} &= \left(U_1/\overline{P}_2\right)|_{U_2=0} = j(Z_0/E_{12})^{-1}\ ,\\ T_{22} &= \left(U_1/U_2\right)|_{\overline{P}_2=0} = E_{22}/E_{12}\ .\end{aligned} \qquad (5)$$

The transmission loss ($TL$) between the inlet (node 1) and outlet (node 2) is expressed as

$$TL{=}20\log[|\,T_{11}{+}T_{12}/Z_2{+}T_{21}Z_1{+}T_{22}(S_2/S_1)|/2\,], \quad (6)_1$$

where

$$Z_1 = \rho_o c/S_1, \qquad Z_2 = \rho_o c/S_2, \qquad S_1 = b_1 h_1, \qquad S_2 = b_2 h_2. \tag{6}_2$$

Consequently, the transmission loss of a straight rectangular muffler is established.

### 2.2. Transmission loss and objective function of a muffler with three rectangular fin-shaped chambers

The mechanism of a muffler with three rectangular fin-shaped chambers is depicted in Fig. 2. According to the mathematical form of a straight rectangular muffler shown in Eq. (6), the four-pole transfer matrix for the muffler between nodes 1 and 6 yields

$$\begin{bmatrix} P_1 \\ U_1 \end{bmatrix} = \prod_{m=1}^{5} [T_m(f)] \begin{bmatrix} P_6 \\ U_6 \end{bmatrix} = \begin{bmatrix} T_{T11} & T_{T12} \\ T_{T21} & T_{T22} \end{bmatrix}, \tag{7}_1$$

$$TL(f, \overline{X}) = 20 \log \left[ \frac{\left| T_{T11} + \frac{T_{T12}}{Z_2} + T_{T21} Z_1 + T_{T22}(S_2/S_1) \right|}{2} \right], \tag{7}_2$$

where

$$\overline{X} = (T1, A0, H0). \tag{7}_3$$

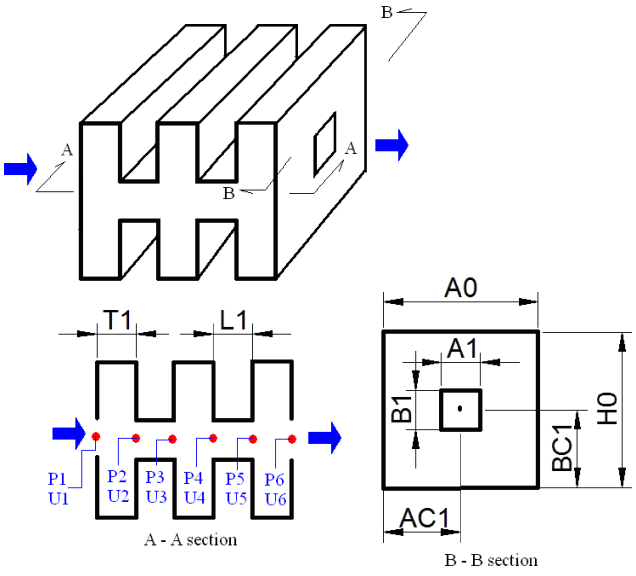


Fig. 2. Mechanism of a multiple-chamber rectangular muffler.

By using the formula of Eq. (7), the objective function used in the *DE* optimization is established as follows:

$$OBJ = TL(f, \overline{X}). \tag{8}$$

Consequently, the transmission and objective function of a muffler with three rectangular fin-shaped chambers are built.

## 3. Model check

Before performing the *DE* optimal simulation on mufflers, a comparison of a rectangular three-chamber muffler with Ih's analytic solution at Bo = Ho = 0.15 m, B1 = B2 = H1 = H2 = 0.05 m, and Lo = 0.025 m is performed and shown in Fig. 3. As depicted in Fig. 3, they are in agreement. Therefore, the proposed mathematical model for a straight rectangular muffler is acceptable. Consequently, the model linked with the numerical method is applied to the shape optimization of a three-rectangular fin-shaped chamber muffler in the following section.

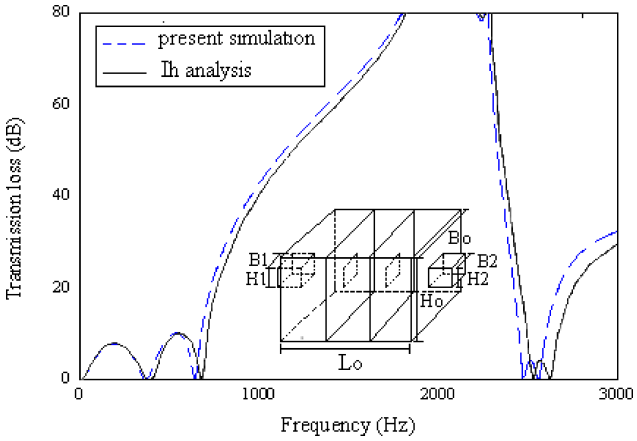


Fig. 3. Comparison of the simulated results of a rectangular three-chamber muffler with Ih's analytic solution (Bo = Ho = 0.15 m, B1 = B2 = H1 = H2 = 0.05 m, Lo = 0.025 m) (Ih, 1992).

## 4. Sensitivity analysis

A three-rectangular chamber fin-shaped muffler is shown in Fig. 2. The related geometric data of the muffler are: A1 = 0.01 m; B1 = 0.01 m; A2 = 0.01 m; B2 = 0.01 m; T1 = 0.01 m; L1 = 0.01 m. In order to understand the influence of the transmission loss with respect to various geometric parameters, a series of acoustical analyses using Eq. (7) is performed and described below.

### 4.1. Varying the thickness of the fin-shaped chamber (T1)

The thickness (T1), including 0.005 m, 0.01 m, and 0.02 m, is adopted in the acoustical simulation for the muffler. As indicated in Fig. 4, the performed adjustment of the thickness (T1) indicates that the profile of transmission loss will be broadened and shifted to the right side when the thickness (T1) of the fin-shaped chamber increases. Obviously, the thickness (T1) with respect to the TL curve is influential.

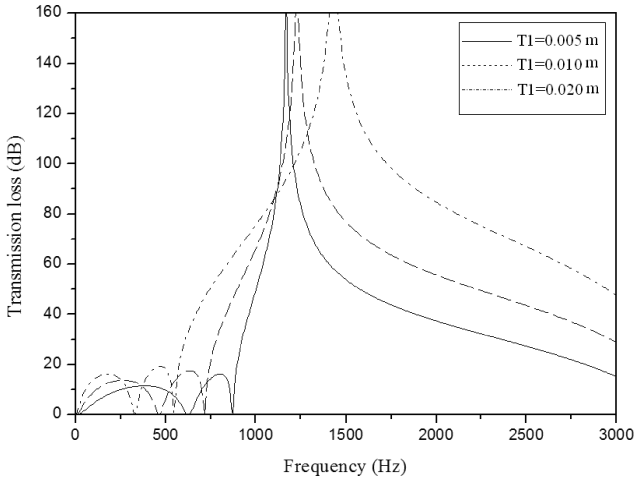


Fig. 4. Response of transmission loss with respect to the design parameter (T1: thickness of the fin-shaped chamber).

### *4.2. Varying the section area of the fin-shaped chamber (A0 ∗ H0)*

The section area (A0 ∗ H0), including

$$0.005 * 0.005 \text{ m}^2, \quad 0.01 * 0.01 \text{ m}^2, \quad \text{and} \quad 0.02 * 0.02 \text{ m}^2,$$

is adopted in the acoustical simulation for the muffler. As indicated in Fig. 5, an adjustment of the section area (A0 ∗ H0) is performed. Figure 5 indicates that the profile of transmission loss will be broadened and shifted to the left side when the section area (A0 ∗ H0) of the fin-shaped chamber increases. Obviously, the increment of the section area (A0 ∗ H0) enhances the noise reduction in lower frequencies. The response of the TL curve with respect to the section area (A0 ∗ H0) is also influential.

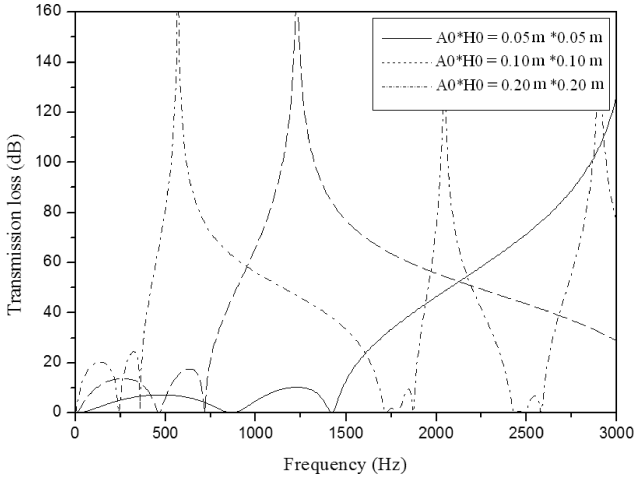


Fig. 5. Response of the transmission loss with respect to the design parameter (A0 ∗ B0: section area of the fin-shaped chamber).

### *4.3. Varying the horizontal distance between the fin-shaped chambers (L1)*

The horizontal distances (L1), including 0.005 m, 0.01 m, and 0.02 m, are adopted in the acoustical simulation for the muffler. As indicated in Fig. 6, an adjustment of the horizontal distance (L1) is performed. Figure 6 indicates that the profile of transmission loss will be broadened when the horizontal distance (L1) of the fin-shaped chamber increases. Obviously, the response of the TL curve with respect to the horizontal distance (L1) is also influential.

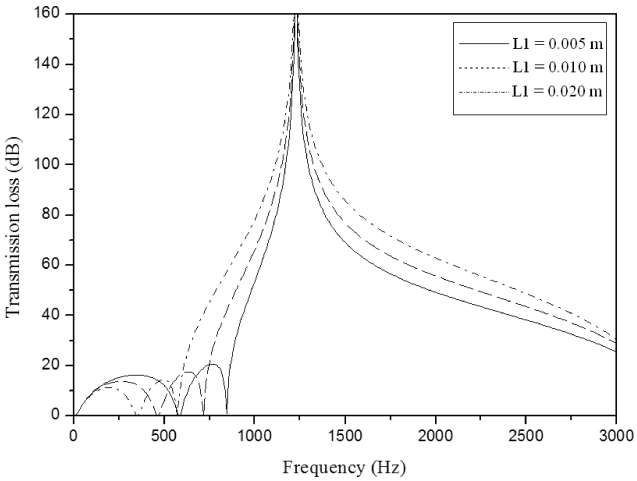


Fig. 6. Response of the transmission loss with respect to the design parameter (L1: horizontal distance between the fin-shaped chamber).

### *4.4. Varying the section area of the inlet/outlet (A1 ∗ B1)*

The section area (A1 ∗ B1), including

$$0.01 * 0.01 \text{ m}^2, \quad 0.02 * 0.02 \text{ m}^2, \quad \text{and} \quad 0.05 * 0.05 \text{ m}^2,$$

is adopted in the acoustical simulation for the muffler. As indicated in Fig. 7, an adjustment of the sec-

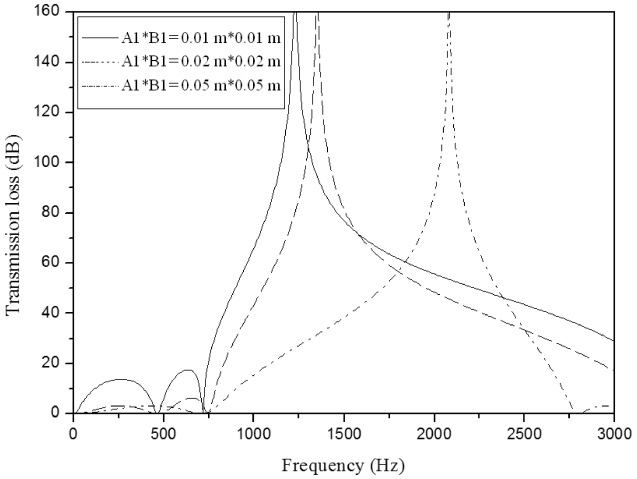


Fig. 7. Response of the transmission loss with respect to the design parameter (A1 ∗ B1: section area of the inlet/outlet).

tion area (A1 ∗ B1) is performed. Figure 7 reveals that the profile of transmission loss will be shifted to the right side when the section area (A1 ∗ B1) of the inlet/outlet increases. Obviously, the increment of the section area (A1 ∗ B1) enhances the noise reduction in higher frequencies. The response of the TL curve with respect to the section area (A1 ∗ B1) is also influential.

## 5. Differential evolution method

The initial population of *DE* will be generated randomly between the lower and upper bounds for each design variable. For a specified population ($NP$), the initial $i$-th design vector ($X_i$) is generated by the random value ($\rho_i$) as

$$X_i = X_{\min} + \rho_i \cdot (X_{\max} - X_{\min}), \quad i = 1, 2, ..., NP, \quad (9)$$

where $\rho_i \in [0, 1]$, $X_{\min}$ and $X_{\max}$ are the minimum and maximum values of the parameters.

The mutation operation of *DE* is executed by multiplying a scaling factor (known as the mutation constant) to a vector difference. Subsequently, a new offspring will be generated by using crossover and selection. For an $m$-dimensional search space and each target vector ($X_{i,g}$), a mutant vector generated by three vectors ($X_{r1,g}$, $X_{r2,g}$, and $X_{r3,g}$) will be randomly selected with the mutant vector ($V_{i,g+1}$) generated using the mutation factor ($F$) as

$$V_{i,g+1} = X_{r1,g} + F \cdot (X_{r2,g} - X_{r3,g}), \quad (10)_1$$

where

$$r1, r2, r3 \in \{1, 2, ...., NP\} \quad (10)_2$$

are randomly chosen integers.

In order to increase the diversity of the perturbed parameter vectors that can expand the searching space during the *DE* operation, a crossover mechanism is used. The trial vector ($U_{i,g+1}$) will be generated via the crossover mechanism between the mutant vector ($V_{i,g+1}$) and the target vector ($X_{i,g}$). Here, the target vector ($X_{i,g}$) is selected from the population. As indicated in Fig. 8, for an $m$-dimensional search space, $X_{ji,g}$ relates to the target vector at the $j$-th parameter and the $i$-th population for the $g$-th generation. The initial target vector can be expressed as

$$X_{i,g} = (X_{1i,g}, X_{2i,g}, X_{3i,g}, ...., X_{ji,g}), \quad j \in [1, m], \quad i \in [1, NP]. \quad (11)$$

The initial mutant vector yields

$$V_{i,g+1} = (V_{1i,g+1}, V_{2i,g+1}, V_{3i,g+1}, ...., V_{ji,g+1}), \quad j \in [1, m], \quad i \in [1, NP]. \quad (12)$$

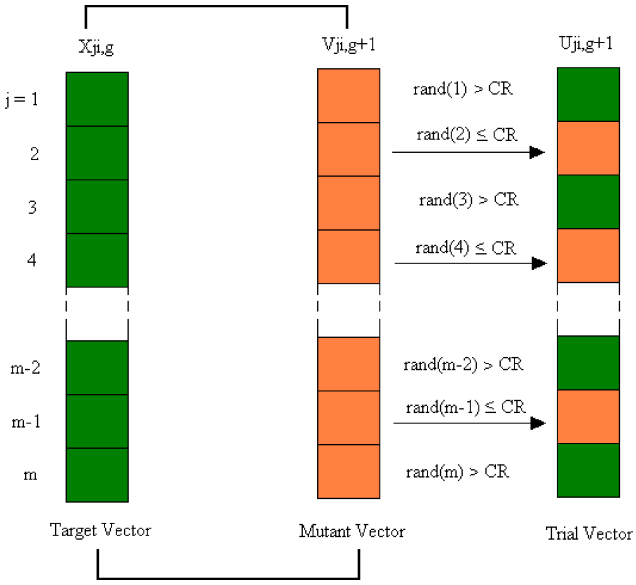


Fig. 8. Mechanism of crossover for a target and mutant vectors in the *DE* method.

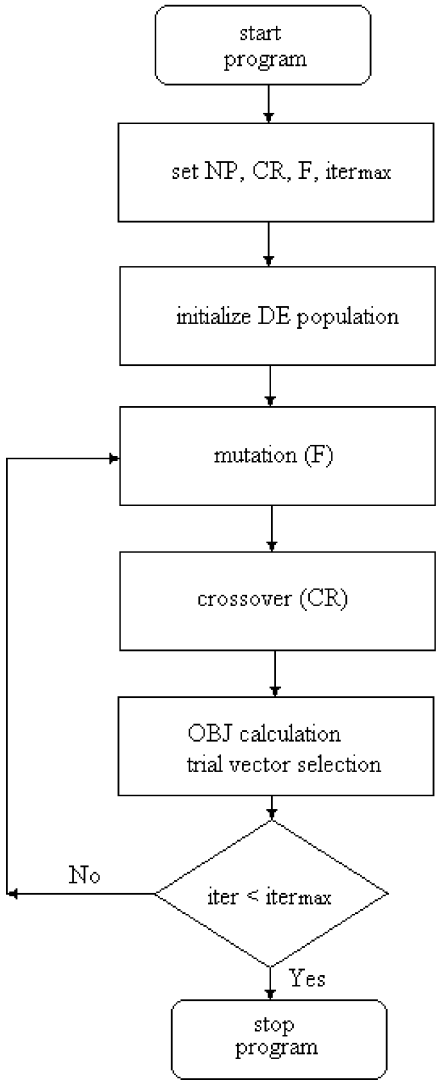


Fig. 9. Flow diagram of the *DE* optimization.

For a $j$-th searching space, the trial vector $(U_{ji,g+1})$ will be conducted using the crossover on the mutant vector $(V_{ji,g+1})$ and target vector $(X_{ji,g})$

$$U_{ji,g+1} = \left[ \begin{array}{l} X_{ji,g} \ldots rand(0,1) > CR \\ V_{ji,g+1} \ldots else \end{array} \right. \\ \left. \ldots j \in [1,m]; \quad i \in [1,NP] \right), \tag{13}$$

where $rand\,(j)$ is between 0 and 1, and $CR$, the crossover constant, is within the range of 0∼1. The new trial vector $(U_{ji,g+1})$ will remain the same as the target vector $(X_{ji,g})$ when a random number $(rand\,(j))$ of rand (0,1) for the $j$-th parameter is greater than a preset $CR$; if not, the new trial vector $(U_{ji,g+1})$ will be replaced by the mutant vector $(V_{ji,g+1})$.

To simplify the numerical assessment when using the *DE* method, a maximal evolution iteration $(iter_{\max})$ is preset. As indicated in Fig. 9, the process will be continually repeated until the predetermined number $(iter_{\max})$ of the outer loop is achieved.

## 6. Results and discussion

### 6.1. Results

The *DE* optimization has four control parameters including $NP$ (population number), $CR$ (crossover rate), $F$ (mutation factor), and $iter_{\max}$ (maximum iteration). Based on the *DE* parameter assessment from Rainer and Kenneth (1996), an appropriate number for population $(NP)$ is preset as $5 * m$ where $m$ is the number of parameters. To achieve a good optimization, the following parameters are varied step by step:

$CR$ (0.1, 0.3, 0.5, 0.7, 0.9);

$F$(0.1, 0.3, 0.5, 0.7, 0.9);

$iter_{\max}$ (50, 100, 500).

According to the sensitivity analysis in Sec. 4, it can be seen that the design parameters T1 and A0 ∗ H0 can largely promote the whole TL curve. In order to exactly design an appropriate design set that will maximize the transmission loss at a specified tone, T1, A0, H0 are adopted as the design parameters during the *DE* optimization.

The range of the design parameters is set as T1: [0.01, 0.02]; A0: [0.10, 0.25]; H0: [0.10, 0.25].

Using Eq. (8), the maximization of the transmission loss with respect to the muffler at the specified pure tone (1000 Hz) was performed first. The optimal design data obtained at $(CR,\ F,\ iter_{\max}) = (0.7,\ 0.1,\ 500)$ are shown in Table 1. Using the optimal design in a theoretical calculation, the optimal transmission $TL$ curves before and after the optimization at a target tone of 1000 Hz is performed are plotted and depicted in Fig. 10.

Table 1. The design parameters and acoustical performance before and after the optimization being performed (optimized at $CR = 0.7$, $F = 0.1$, $iter_{\max} = 100$).

| | Design parameters | | | STL [dB] |
|---|---|---|---|---|
| | T1 [m] | A0 [m] | H0 [m] | |
| Original at 1000 Hz | 0.010 | 0.100 | 0.100 | 64 |
| Optimization at 1000 Hz | 0.018 | 0.128 | 0.128 | 160 |
| Original at 2500 Hz | 0.010 | 0.100 | 0.100 | 43 |
| Optimization at 2500 Hz | 0.018 | 0.168 | 0.168 | 110 |
| A1 = 0.01 (m); B1 = 0.01 (m); L1 = 0.01 (m) | | | | |

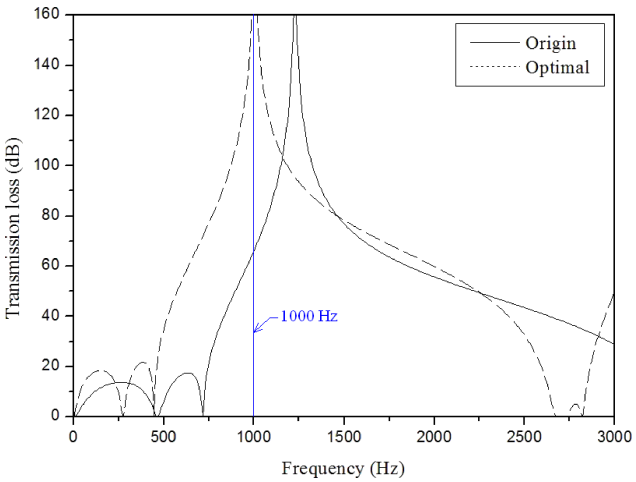


Fig. 10. Comparison of the optimal and original TLs at a target tone of 1000 Hz.

Similarly, using the same *DE* control parameter set of $(CR,\ F,\ iter_{\max}) = (0.7,\ 0.1,\ 500)$, the optimization at a target tone of 2500 Hz is carried out. The related design data and related $TL$ at the target tone of 2500 Hz are also illustrated in Table 1. Using the optimal design in a theoretical calculation, the optimal transmission $TL$ curves before and after the optimization at a target tone of 2500 Hz are plotted and depicted in Fig. 11.

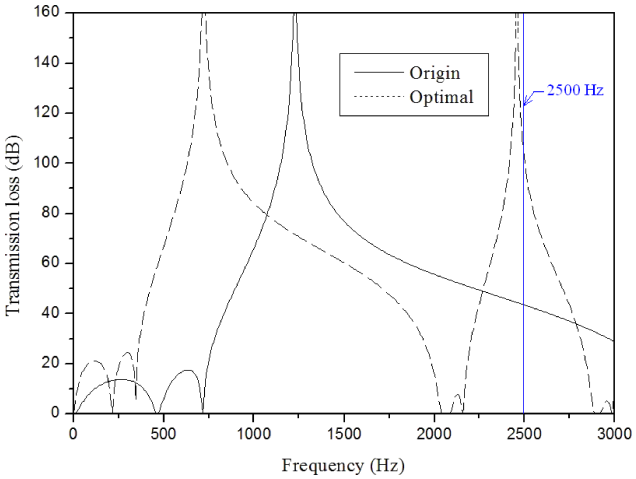


Fig. 11. Comparison of the optimal and original TLs at a target tone of 2500 Hz.

### 6.2. Discussion

To achieve a sufficient optimization, the selection of the appropriate *DE* parameter set is important. As indicated in Table 1, concerning the target frequency of 1000 Hz, the *TL* of the muffler at 1000 Hz can be improved from 64 dB to 160 dB. As it can be seen in Fig. 10, the predicted maximal value of the *TL* is exactly located at the desired frequency. Therefore, the reliability of the *DE* optimizer used in the optimization of the mufflers is assured.

Moreover, in dealing with the target tone of 2500 Hz, the resulting design data and related TL before and after the optimization being performed indicates that the TL at a target tone of 2500 Hz can be improved from 43 dB to 110 dB. As can be seen in Fig. 11, the predicted maximal value of the *TL* is roughly located at the desired frequency of 2500 Hz.

## 7. Conclusion

It has been shown that three kinds of *DE* parameters (*CR*, *F*, and $iter_{\max}$) play vital roles in the solution's accuracy during the *DE* optimization. As discussed in the sensitivity analysis in Sec. 4, the design parameters of T1, A0, H0 can tremendously influence the muffler's acoustical performance. The optimization of muffler shapes within a limited space can be easily and efficiently carried out by using the eigenfunction in conjunction with a four-pole transfer matrix as well as a *DE* optimizer. As indicated in Figs. 10 and 11, the predicted maximal value of the *TL* is roughly located at the desired frequency. The results reveal the transmission loss can be improved by 96 dB when using a target tone of 1000 Hz. Also, using a target tone of 2500 Hz, the improvement of the *TL* can reach 67 dB after the optimization process is performed.

Consequently, the approach used for the shape optimization in the specified tones using a space-constrained muffler composed of three fin-shaped chambers proposed in this study is important and can be efficiently accomplished.

## References


1. Abom M. (1990), *Derivation of four-pole parameters including higher order mode effects for expansion chamber mufflers with extended inlet and outlet*, Journal of Sound and Vibration, **137**, 403–418.
2. Chang Y.C., Chiu M.C. (2014), *Optimization of rectangular multi-chamber plenums equipped with extended tubes using the BEM, neural networks, and genetic algorithm*, J. of Mechanics, **30**, 6, 571–584.
3. Chang Y.C., Yeh L.J., Chiu M.C. (2004), *Optimization of constrained multi-layer absorbers by using genetic algorithms*, International Journal of Acoustics and Vibration, **9**, 4, 175–185.
4. Chang Y.C., Yeh L.J., Chiu M.C., Lai G.J. (2005), *Shape optimization on constrained single-layer sound absorber by using GA method and mathematical gradient methods*, Journal of Sound and Vibration, **1286**, 4–5, 941–961.
5. Chiu M.C. (2014), *Numerical assessment of rectangular side inlet/outlet plenums internally hybridized with two crossed baffles using a FEM, neural network, and GA method*, J. of Low Frequency Noise, Vibration and Active Control, **33**, 3, 271–288.
6. Chiu M.C. (2010), *Shape optimization of multi-chamber mufflers with plug-inlet tube on a venting process by genetic algorithms*, Applied Acoustics, **71**, 495–505.
7. Chiu M.C., Chang Y.C. (2008), *Numerical studies on venting system with multi-chamber perforated mufflers by GA optimization*, Applied Acoustics, **69**, 11, 1017–1037.
8. Chiu M.C., Chang Y.C. (2013), *Numerical Assessment of plenums intersected with four baffles using the boundary element method, genetic algorithm, and the neural networks*, Noise & Vibration Worldwide, **44**, 11, 25–44.
9. Chiu M.C., Chang Y.C. (2014) *An assessment of high-order-mode analysis and shape optimization of expansion chamber mufflers*, Archives of Acoustics, **39**, 4, 489–499.
10. Igarashi J., Toyama M. (1958), *Fundamentals of acoustical silencers, part 1: Theory and experiment of acoustic low-pass filters*, Aeronaut Res. Inst. University of Tokyo, Report No. **339**, 223–241.
11. Igarashi J., Arai M. (1960), *Fundamentals of acoustical silencers, part 3: attenuation characteristic studies by electric simulator*, Aeronaut Res. Inst. University of Tokyo, Report No. **351**, 17–31.
12. Ih J.G., Lee B.H. (1985), *Analysis of higher-order mode effects in the circular expansion chamber with mean flow*, Journal of the Acoustical Society of America, **77**, 1377–1388.
13. Ih J.G., Lee B.H. (1987), *Theoretical prediction of the transmission loss of circular reversing chamber mufflers*, Journal of Sound and Vibration, **112**, 261–272.
14. Ih J.G. (1992), *The reactive attenuation of rectangular plenum chambers*, Journal of Sound and Vibration, **157**, 93–122.
15. Miwa T., Igarashi J. (1959), *Fundamentals of acoustical silencers, part 2: Determination of four terminal constants of acoustical element*, Aeronaut Res. Inst. University of Tokyo, Report No. **344**, 67–85.
16. Munjal M.L. (1987), *A simple numerical method for three-dimensional analysis of simple expansion chamber mufflers of rectangular as well as circular cross-*

*section with a stationary medium*, Journal of Sound and Vibration, **116**, 71–88.

17. Rainer S., Kenneth P. (1996), *Minimizing the real functions of the ICEC'96 contest by differential evolution*, IEEE Evolutionary Computation Conference, Nayoya, Japan, 842–844.

18. Seybert A.F., Cheng C.Y.R. (1987), *Application of the boundary element method to acoustic cavity response and muffler analysis*, Transactions of the American Society of Mechanical Engineers, Journal of Vibration, Stress, and Reliability in Design, **109**, 15–21.

19. Storn R., Price K. (1995), *Differential evolution – a simple and efficient adaptive scheme for global optimization over continuous space*, Technical Report TR-95-012, 1995.

20. Storn R., Price K. (1997), *Differential evolution – a simple and efficient heuristic for global optimization over continuous spaces*, Journal of Global Optimization, **11**, 341–359.

21. Yeh L.J., Chang Y.C., Chiu M.C., Lai G.J. (2004), *GA optimization on multi-segments muffler under space constraints*, Applied Acoustics, **65**, 5, 521–543.

22. Young C.I., Crocker M.J. (1975), *Prediction of transmission loss in mufflers by the finite-element method*, Journal of the Acoustical Society of America, **57**, 144–148.